Optics Letters

Optically pumped lasing with a Q-factor exceeding 6000 from wet-etched GaN micro-pyramids

L. C. Wang,[1,2,7,*] Y. Y. Zhang,[6] R. Chen,[4] Z. Q. Liu,[2,3] J. Ma,[2] Z. Li,[2] X. Y. Yi,[2,3,8] H. J. Li,[5] J. X. Wang,[2,3] G. H. Wang,[2,3] W. H. Zhu,[1,9] and J. M. Li[2,3]

[1]College of Mechanical and Electrical Engineering, State Key Laboratory of High Performance Complex Manufacturing, Central South University, Changsha Hunan 410083, China
[2]Semiconductor Lighting Technology Research and Development Center, Institute of Semiconductors, Chinese Academy of Sciences, Beijing 100083, China
[3]College of Materials Science and Opto-Electronic Technology, University of Chinese Academy of Sciences, Beijing 101408, China
[4]Department of Electrical and Electronic Engineering, South University of Science and Technology of China, Shenzhen, Guangdong, 518055, China
[5]Department of Materials Science and Engineering, University of California, Santa Barbara, Santa Barbara, California 93106, USA
[6]Department of Electrical Engineering and Computer Science, Northwestern University, Evanston, Illinois 60208, USA
[7]Mind Star (Beijing) Technology Co., Ltd., Zhongguancun South Street, Haidian District, No. 45 Hing Fat Building 1001, Beijing 100872, China
[8]e-mail: spring@semi.ac.cn
[9]e-mail: zhuwenhui@csu.edu.cn
*Corresponding author: wanglc@semi.ac.cn

Received 14 June 2017; accepted 29 June 2017; posted 3 July 2017 (Doc. ID 298006); published 25 July 2017

We report the observation of room-temperature optically pumped lasing modes from a single GaN pyramid microcavity on a metallic mirror. The mode at 367.2 nm exhibits a low threshold (0.4–0.5 MW/cm^2) and a narrow linewidth (0.054 nm), by which the quality factor can be estimated to be >6000. These lasing behaviors can be attributed to the specific wet-etching approach by selectively etching away defects and pyramid geometry with bottom Ag reflectors for better light confinement. Optical resonances in these pyramids are further investigated in combination with three-dimensional finite-difference time-domain simulations.

OCIS codes: (230.0230) Optical devices; (250.0250) Optoelectronics; (120.4610) Optical fabrication.

https://doi.org/10.1364/OL.42.002976

Nitride based microcavities have attracted intensive interest due to the physical insight of lasing mechanisms in both the weak and strong coupling regimes [1,2] (for example, photon–exciton or polariton dynamics and its coherent state polariton lasing) and their widespread applications [3]. Different geometrics of nitride-based optical microcavities have been demonstrated and investigated for achieving high-quality lasing, such as Fabry–Perot resonators [4], defective photonic crystal structures [5], and microdisks via whispering-gallery modes (WGMs) [6–10]. The performance of III-nitride microcavity lasers has been greatly limited by material qualities, processing techniques, and significant optical loss caused by optical coupling to the sapphire substrate or through rough sidewalls [1–9,11–13]. Here we report the observation of room temperature optically pumped lasing modes from a single pyramid GaN microcavity. The pyramid GaN microcavity exhibits several distinctive features, compared with the above mentioned GaN microcavity counterparts. First, these pyramid microcavities are fully wet etching accessed; thus, the material defects are partially etched away, and relatively smooth crystalline facets have been obtained. The smooth crystalline facets exposed in the wet-etching process will reduce the leakage for the optical resonance confined by reducing the light-scattering loss at the GaN/air interface. Second, these pyramids will facilitate the formation of standing waves due to the hexagonal geometry, so called "quasi-WGMs". Moreover, high reflectance metallic mirrors at the bottom of the pyramid microcavities will enhance optical confinement in the vertical direction. Riding on these advantages, multiple lasing modes are observed. Specifically, for example, the lasing mode observed at a wavelength of 367.2 nm exhibits a low threshold (0.4 – 0.5 MW/cm^2), a high quality (Q)-factor (over 6000), and a narrow linewidth (0.054 nm). To identify the optical modes observed in the photoluminescence (PL) spectra, we also conduct three-dimensional (3D) finite-difference time-domain (FDTD) simulations using commercial Lumerical FDTD solutions and comprehensively analyze these pyramid-shaped GaN microcavities.

Figure 1 sketches the fabrication process of the vertical pyramid GaN microcavity. The nitride-based thin film is epitaxially grown on sapphire substrate using a metal organic chemical vapor deposition (MOCVD) method, consisting of a 2 μm unintentionally doped GaN layer (u-GaN). After the epitaxial growth

procedure, a Ni/Ag/Pt/Au (0.2/300/10/300 nm) metallic reflector is deposited on u-GaN using an electron-beam evaporator. Afterwards, 100 μm copper (Cu) is electroplated on the metallization contact as the new substrate. Then the separation of the GaN thin-film from the sapphire substrate is achieved through a laser lift-off (LLO) process using a 248 nm K_rF laser system. The transferred GaN epitaxial film is wet-etched thoroughly until the randomly distributed vertical pyramid GaN microcavities are obtained. Here dilute potassium hydroxide (KOH) solution with a concentration of 6 mol/L is adopted as the etchant at a constant temperature of 70°C in a water bath. When the etching process is finished, the sample is rinsed in DI water. The sample is placed on a sample holder mounted on an X-, Y-, and Z-movable stage. The signal emitted from an individual pyramid was collected with a UV objective, focused into an optical fiber, and directed into a 750 mm monochromator combined with a UV-enhanced back-illuminated charged-coupled device for spectral recording.

Figure 1(b) shows a tilted-view SEM image of the single GaN pyramid obtained from the wet-etching process, with the base radius and height around 1.2 and 2.1 μm, respectively. Some particles are observed on the bottom part of the pyramid investigated, which are considered to be the chemical reaction products, such as the Ga droplets and its compounds. They will cause scattering loss in some incidences on these areas, degrading the performance or even preventing the occurrence of the corresponding lasing. However, we will demonstrate later that the observed lasing modes most probably stem from the incidences on the top part of the pyramid; thus, the particles on the bottom should have limited influence on the characteristics of these lasing modes. These contaminants can be removed by increasing both the HCl solution, together with the ultrasonic treatment. Figure 2 shows the PL spectra of the single vertical pyramid measured by varying the peak power density of optical pumping from 0.06 to 0.8 MW/cm^2. A broad emission peak with full width at half-maximum of approximately 12.3 nm at around 369.7 nm is observed, corresponding to the typical spontaneous near band-edge emission from the u-GaN pyramid. When the optical pumping power density increases, other peaks at the high-energy side emerge at around 367.2 and 368.4 nm, respectively. With further increasing of the optical pumping power density, these peaks become narrower and stronger, indicating an onset of the stimulated emission process. The Inset of Fig. 2 demonstrates that the peak wavelengths for modes M_1, M_2, and M_3 are located at 367.2, 368.4, and 369.6 nm, respectively, and all exhibit negligible shift (0.1 nm) versus excitation power densities. The mode

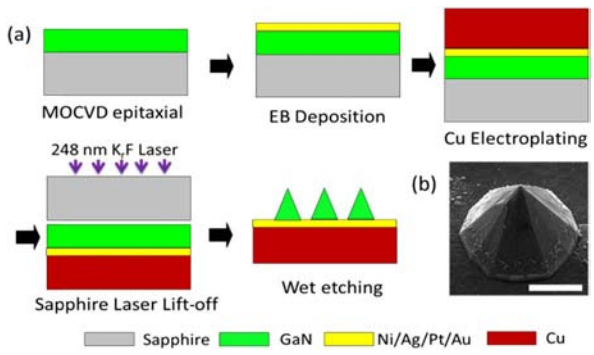

Fig. 1. (a) Fabrication process of the vertical pyramid GaN microcavity; (b) SEM image of a single GaN pyramid. Scale bar: 1 μm.

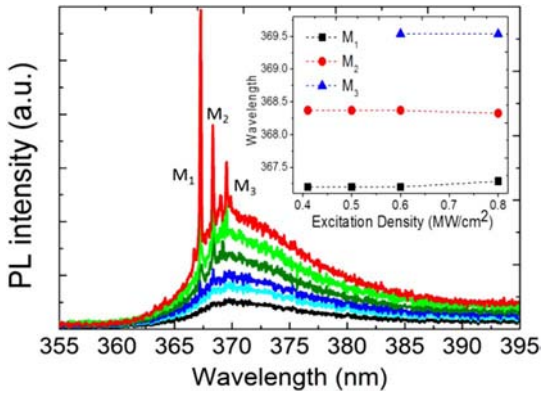

Fig. 2. PL spectra of a single vertical pyramid measured with varying pumping power densities. The inset shows the peak wavelength variation for the modes M_1, M_2, and M_3 versus excitation power densities.

spacing between M_1, M_2, and M_3 modes is 1.2 nm. Figure 3(a) shows the integrated PL intensities of the spectral modes at 367.2 and 368.4 nm as a function of excitation power density. Under low excitation power densities, the integrated intensity increases linearly with increasing excitation power density. For M_1, a nonlinear increase in integrated intensity has been observed when the excitation power density exceeds 0.4 and 0.3–0.5 MW/cm^2. Simultaneously, as shown in Fig. 3(b), the linewidth shows a dramatic reduction to 0.054 nm at 0.6 MW/cm^2, which is near the resolution of the measurement equipment. As the optical pumping density further increases, the linewidth increases slightly due to free electron absorption and the electron-hole plasma effect [14]. A sublinear increase in the integrated intensities for M_2 is also observed, which is due to the mode competition. We think both the nonlinear increase in intensity and the dramatic reduction in the linewidth confirm the lasing characteristics, and the threshold (labeled as E_{th}) for optically pumped lasing can be roughly estimated to be 0.4–0.5 MW/cm^2. The Q-factor is an important parameter to evaluate the quality of a laser cavity. From the M_1 mode at 367.2 nm, the Q-factor is estimated to be as high as 6070 at the threshold according to the definition $Q = \lambda/\ \lambda$, where λ is the peak wavelength and λ is the linewidth of the peak, respectively. Furthermore, 3D-FDTD simulations over a wavelength region from 355 to 395 nm have been conducted to analyze the mode characteristics. In the simulation, the dipoles are randomly placed at the xy-plane

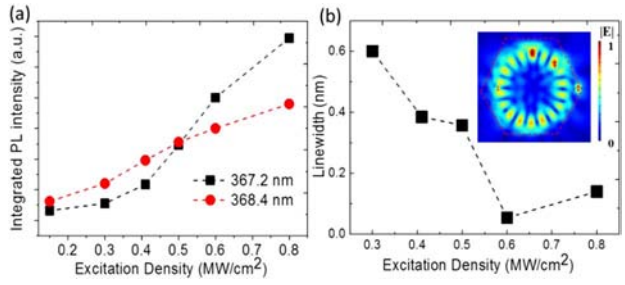

Fig. 3. (a) PL integrated intensity of optical modes at 367.2 and 368.4 nm as a function of excitation power density; (b) the linewidth evolution of mode at 367.2 nm versus pumping excitation densities. Inset of (b): FDTD simulated cross-sectional electric-field energy intensity pattern of TE1,18 around 365 nm.

200 nm above the base of the modeled pyramid cavity with a diameter of 2.4 μm, consistent with the size obtained from the SEM observation, andone-plane monitors are placed at the xy-plane to plot the $|E|$ distributions in the pyramid horizontal direction. The n_{eff} of the GaN pyramid is set to 2.65, based the theoretical refractive index value at around 365 nm. Based on simulation results, the dominant lasing peak at 365 nm can be attributed to a first-order ($n = 1$) transverse-electric (TE) mode ($m = 18$). The xy-plane electric-field energy intensity pattern of TE1,18 around 365 nm is plotted in the inset of Fig. 3(b). The regions shaded in red and blue represent the highest and lowest field intensities, respectively, whereas the micro-pyramid top-view boundary is defined by the red dashed line. It should be pointed out that, practically, the whole pyramid acts as the active area, and light is emitted everywhere from the pyramid; yet, this cannot be fully implemented in the simulations. Here the dipole sources are only placed at a single horizontal plane. The simulation result shown here only renders possible resonant modes from the pyramid microcavity. It demonstrates that the mode of the lasing observed shows quasi-WGM characteristics. Moreover, it is found that the bottom Ag reflector plays a significant role for sustaining the lasing mode, since the lasing characteristics are absent when Ag is removed in the simulation.

Lasing phenomena could not happen without appropriate cavity feedback. Various feedback mechanisms may account for the lasing, such as a random resonant effect, F–P resonances, or WGMs. In our experiment, since the lasing is observed from a single GaN pyramid and is far away from other pyramids, it cannot be attributed to random lasing caused by multiple scattering in a disordered medium. F–P resonances are not possible in the micro-pyramid either because of the absence of two paralleled facets. Actually, we think the specific pyramid geometry can serve as the special microcavity for circulating the light inside it. In particular, the pyramid-shaped GaN cavity can also support quasi-WGMs, where the light is totally reflected by the six lateral facets with an incident angle of 58.4° and the bottom Ag. Bidnyk *et al.* [15] and Jiang *et al.* [16] previously reported and analyzed the optical resonant modes in GaN pyramids microcavities. In contrast to our approach, the GaN pyramids are obtained by selective epitaxial overgrowth. Figures 4(a) and 4(b) sketch two types of possible light propagating paths within the vertical pyramid microcavity. The first type can be identified easily from the 3D configuration in Fig. 4(a): two opposite facets, such as the JAB and JED planes together, with the metallic mirror at the bottom, forming one cavity, and the red line is one possible propagating light beam path. Figures 4(a-i) and 4(a-ii) further sketch the vertical cross-sectional view of two specific light propagating paths belonging to the first type of resonance, whereas points H and I are the center points of line AB and line DE, respectively. Take Fig. 4(a-i) as the example; light (red arrow line) propagating in a direction with a specific angle to plane JAB will be reflected to plane JED (line VW) and further reflected to original point U at the base plane (line WU). A standing mode forms if the phase condition matches. Higher-order modes are also possibly supported by this cavity with multiple reflections, as sketched in Fig. 4(a-ii). We refer to the first type of modes as vertical quasi-WGMs. Alternatively, for the second type of resonator, light can be multiply reflected between the triple or the six sidewall facets and the bottom of the pyramids in a zigzag way, as depicted in Fig. 4(b). Figures 4(b-i) and 4(b-ii) sketch horizontal cross-sectional views of two specific light propagating paths belonging to the second type of resonance. The circulating path for the simplest mode is illustrated as an example, as shown in Fig. 4(b-i): a light beam SO from the basal plane incidents to one of the sidewall facet JAB to point O and bounces back to the basal plane (light OR); then the process repeats, following the optical paths of RQ, QT, and TP, and, finally, back to the original point (line PS). Note that points O, P, and Q are located at the same horizontal plane above, whereas points R, S, and T belong to the base plane of the pyramid. These second type of modes are referred to as horizontal quasi-WGMs and can explain the multiple modes observed in the spectral in Fig. 2. Since the reflection at the GaN/air sidewalls and the total absorption varies at the different incident angles and for the light path length for different modes, the characteristics for each mode, such as E_{th}, linewidth and Q value, varies.

Jiang *et al.* [16] observed the multiple optical modes from pyramids and has classified them into three different groups with different mode spacings of 1, 0.5, and 0.6 nm. To quantitatively analyze the modes, the mode spacings (λ) were further used to calculate the effective optical path length L by the following Eq. (1):

$$\lambda = \frac{\lambda^2}{L \cdot \left(n - \lambda \frac{dn}{d\lambda}\right)}. \tag{1}$$

Here n is the refractive index of the GaN. The dispersion factor $dn/d\lambda$ can be neglected, and L is the effective optical length. The modes M_1, M_2, and M_3 observed in our pyramid's spectra in Fig. 2 exhibit spacing of 1.2 nm. If M_1, M_2, and M_3 belong to the same modal family, i.e., $\lambda = 1.2$ nm, then L is calculated to be 41.9 μm. Considering the azimuth mode distribution according to the FDTD simulation in the inset of Fig. 3(b), the lateral unit optical length (L_u) is around 2.3 μm. We define the lateral unit length L_u as the optical length for the light path from the basal plane to the sidewall. For example, for the mode with an azimuth number of 3 [Fig. 4(b-i)], the lateral unit length is equal to SO. Further we can observe that the modal energy is mostly confined in the inner circle of the base hexagonal plane. Thus, the inclined angle between line SO and the basal plane is estimated to be 82.4° ($\arccos[(2\pi r/m)/L_u]$, where r is the inner radius of the base hexagonal plane and m is the azimuth number of mode), indicating that the observed modes in Fig. 2 are mostly incident

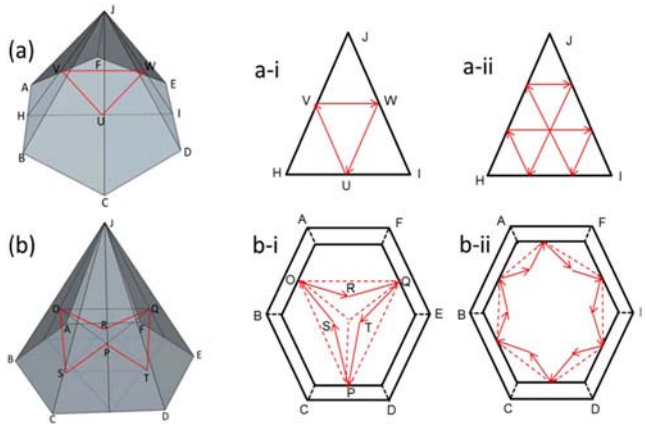

Fig. 4. (a) and (b) Sketches of two types of possible light propagating paths within the vertical pyramid microcavity.

vertically and most probably impinge on the top part of the pyramids. Alternatively, if $\lambda = 2.4$ and 3.6 nm, then L is calculated to be 21 and 14 μm, and the corresponding inclined angle is 75° and 67°, respectively. Considering that the radius of the pyramid in Ref. [16] and our experiment is 8 and 1.2 μm, respectively, a modal spacing of 3.6 nm for our pyramid, counterpart to modal spacing of 0.5 nm in Ref. [16], is reasonable. Nonetheless, in all situations, it is reasonable to consider that the particles observed in the bottom part of the pyramid investigated shown in Fig. 1(b) cause negligent light scattering loss for the observed lasing modes. The single vertical pyramid GaN sits on top of the Ag reflector and is obtained through sufficient etching in KOH from the N-polar surface. Our previous studies have shown that the wet-etching process can filter, i.e., selectively etch away part of the material defects, resulting in improved crystal quality of the pyramid [17,18]. Furthermore, the sidewall morphologies of the wet-etching obtained pyramid facets can be quite smooth, whereas the boundary imperfections and sidewall roughness are inevitable for a conventional dry-etching approach. These are favorable to an enhanced inherent material gain and optical confinement, thus leading to the observation of lasing. Initially, the performances of III-nitride microdisk lasers have been greatly limited by significant optical loss caused by optical coupling to the sapphire substrate. Thus, it is necessary to obtain an undercut structure to enhance optical vertical confinement through a special epitaxial structure design and wet-etching approach [7]. The bottom Ag reflector metal (Ni/Ag/Pt/Au) could avoid the complicated undercut process, and its high reflectance provides optical vertical confinement and aids the lasing.

Optically pumped lasing actions on various GaN microcavities have been reviewed in Ref. [7]. We further compare the lasing characteristics of reported pyramid microcavities and vertical disk microcavities. Structures reported in Refs. [13,14] show similar pyramid geometry, and a much larger size, the E_{th} ($E_{th} = 25$ MW/cm^2), is 10-fold higher than our reported vertical pyramid. Furthermore, the Q-factor of our vertical pyramid (6000) is much higher, compared with the vertical disk counterpart for WGM lasing reported by Choi [9,19], with Q-factors to be 1673 and 770 for Ag and ITO at the bottom, respectively. This should be attributed to the improved material quality of our pyramid due to the "defects' filter effect" [20], relatively smoother surface morphology, the specific isolated micro-pyramid cavity configuration via the wet-etching process, and the bottom metal reflectance for vertical confinement. Aharonovich [21] and Guillet *et al.* [22] reported high-Q optically pumping room-temperature undercut microdisk lasing in the blue spectral (Q 6600) and UV range (Q 7300), respectively. Compared with the undercut route, another advantage inherent to our reported vertical pyramid structure is that electrically driven lasing can be potentially achieved with the bottom Ag as a bottom electrode. Admittedly, it is difficult to obtain large area isolated pyramids with uniform size using the above lithography-free wet-etching method [23], which is disadvantageous and hurdles further development and its real application. In addition, the development of an improved and more time-efficient wet-etching recipe and approach is necessary.

To conclude, we report the observation of room temperature optically pumped multiple lasing modes from a high-quality single vertical pyramid GaN microcavity. The mode at 367.2 nm exhibits a low threshold (0.4–0.5 MW/cm^2), a high Q-factor (6070), and a narrow linewidth (0.054 nm). This is attributed to the specific wet-etching approach for a defect selective etching effect and vertical pyramid geometry for light confinement. The modes are analyzed with FDTD simulation and discussed both qualitatively and quantitatively. The vertical pyramid represents a definitely new GaN microcavity configuration, and our report initiates a new avenue for GaN microcavity laser fabrication; thus, this Letter is meaningful for the future development of GaN microcavity light emitters, including micro-light-emitting diodes, pixel emitter elements, and microcavity lasers.

Funding. National Key R&D Program of China (2016YFB0400102); National Natural Science Foundation of China (NSFC) (U1505253, 11574130); State Key Development Program for Basic Research of China-973 Program (2015CB057200); Central South University (CSU).

REFERENCES

1. S. Christopoulos, G. Baldassarri Höger Von Högersthal, A. J. D. Grundy, P. G. Lagoudakis, A. V. Kavokin, J. J. Baumberg, and G. Christmann, Phys. Rev. Lett. **98**, 126405 (2007).
2. R. Butté, G. Christmann, E. Feltin, J. F. Carlin, M. Mosca, M. Ilegems, and N. Grandjean, Phys. Rev. B **73**, 033315 (2006).
3. G. Christmann, R. Butté, E. Feltin, A. Mouti, P. A. Stadelmann, A. Castiglia, and N. Grandjean, Phys. Rev. B **77**, 085310 (2008).
4. J. C. Johnson, H. J. Choi, K. P. Knutsen, R. D. Schaller, P. Yang, and R. J. Saykally, Nat. Mater. **1**, 106 (2002).
5. H. Matsubara, S. Yoshimoto, H. Saito, Y. Jianglin, Y. Tanaka, and S. Noda, Science **319**, 445 (2008).
6. S. Chang, N. B. Rex, R. K. Chang, G. Chong, and L. J. Guido, Appl. Phys. Lett. **75**, 166 (1999).
7. Y. Zhang, X. Zhang, K. H. Li, Y. F. Cheung, C. Feng, and H. W. Choi, Phys. Status Solidi A **212**, 960 (2015).
8. Y. Zhang, C. Feng, T. Wang, and H. W. Choi, Appl. Phys. Lett. **108**, 031110 (2016).
9. X. Zhang, Y. F. Cheung, Y. Zhang, and H. W. Choi, Opt. Lett. **39**, 5614 (2014).
10. R. Chen, B. Ling, X. W. Sun, and H. D. Sun, Adv. Mater. **23**, 2199 (2011).
11. E. D. Haberer, R. Sharma, C. Meier, A. R. Stonas, S. Nakamura, S. P. DenBaars, and E. L. Hu, Appl. Phys. Lett. **85**, 5179 (2004).
12. D. Simeonov, E. Feltin, A. Altoukhov, A. Castiglia, J.-F. Carlin, R. Butté, and N. Grandjean, Appl. Phys. Lett. **92**, 171102 (2008).
13. Y. Zhang, Z. Ma, X. Zhang, T. Wang, and H. W. Choi, Appl. Phys. Lett. **104**, 221106 (2014).
14. F. Jahnke, M. Kira, S. W. Koch, G. Khitrova, E. K. Lindmark, T. R. Nelson, Jr., D. V. Wick, J. D. Berger, O. Lyngnes, H. M. Gibbs, and K. Tai, Phys. Rev. Lett. **77**, 5257 (1996).
15. S. Bidnyk, B. D. Little, Y. H. Cho, J. Krasinski, J. J. Song, W. Yang, and S. A. McPherson, Appl. Phys. Lett. **73**, 2242 (1998).
16. H. X. Jiang, J. Y. Lin, K. C. Zeng, and W. Yang, Appl. Phys. Lett. **75**, 763 (1999).
17. L. Wang, J. Ma, Z. Liu, X. Yi, G. Yuan, and G. Wang, J. Appl. Phys. **114**, 133101 (2013).
18. J. Ma, L. Wang, Z. Liu, G. Yuan, X. Ji, P. Ma, and J. Li, Opt. Express **21**, 3547 (2013).
19. X. Zhang, H. Chap, and H. W. Choi, Jpn. J. Appl. Phys. **56**, 01AD04 (2016).
20. H. Dong, Y. Liu, S. Sun, J. Li, J. Zhan, Z. Chen, and L. Zhang, Sci. Rep. **6** (2016).
21. I. Aharonovich, A. Woolf, K. J. Russell, T. Zhu, N. Niu, H. Kappers, and E. L. Hu, Appl. Phys. Lett. **103**, 021112 (2013).
22. T. Guillet, M. Mexis, S. Sergent, D. Neel, S. Rennesson, C. Brimont, T. Bretagnon, B. Gil, D. Sam-Giao, B. Gayral, and F. Semond, Phys. Status Solidi B **249**, 449 (2012).
23. L. Wang, J. Ma, Z. Liu, X. Yi, H. Zhu, and G. Wang, ACS Photon. **1**, 421 (2014).